Proceedings of the 9th U.S. National and 10th Canadian Conference on Earthquake Engineering
Compte Rendu de la 9ième Conférence Nationale Américaine et
10ième Conférence Canadienne de Génie Parasismique
July 25-29, 2010, Toronto, Ontario, Canada • Paper No 969

SATELLITE OBSERVATIONS OF LANDSLIDES CAUSED BY THE 2008 WENCHUAN EARTHQUAKE IN CHINA

Ellen M. Rathje[1] and Lucas P. Carr[2]

ABSTRACT

Pre- and post-event satellite imagery was used to identify landslides and urban damage in the area affected by the 2008 Wenchuan Earthquake in China. LANDSAT imagery at lower spatial resolution was used to analyze landslide patterns across the entire affected area, with landslide mapping being performed over nearly 16,000 km^2. High spatial resolution IKONOS and Quickbird imagery were used to analyze landslide patterns and urban damage in localized areas of intense damage and to validate the findings of the LANDSAT analysis. The relationship between the landslide patterns, geology, and topography was also investigated.

Introduction

Earthquake-induced landslides represent a significant earthquake hazard. Rapid assessments of the landslide distribution after an earthquake can be obtained from satellite imagery. Additionally, these landslide distributions can be used in ongoing research efforts to improve our models that predict earthquake-induced landslides.

The May 12, 2008 Wenchuan Earthquake ($M_w = 7.9$) in China devastated a large region in Sichuan Province, with earthquake-induced landslides representing one of the main mechanisms of damage. The large area affected by the earthquake makes it difficult to identify the landslide distribution via traditional methods. Pre- and post-event satellite imagery was used in an effort to identify landslides, as well as urban damage, across the region affected by the earthquake. LANDSAT imagery at lower spatial resolution was used to analyze landslide patterns across the entire affected area, with landslide mapping being performed over nearly 16,000 km^2. High spatial resolution IKONOS and Quickbird imagery were used to analyze landslide patterns and urban damage in localized areas of intense damage and to validate the findings of the LANDSAT analysis. The relationship between landslide patterns, geology, and topography was also investigated.

---

[1]Professor, Dept. of Civil, Architectural, and Environmental Engineering, University of Texas, Austin, TX 78712
[2]Staff Engineer, URS Corporation, St. Louis, MO 63110

IMAGERY AVAILABLE

Four LANDSAT scenes encompass the immediate area affected by the Wenchuan Earthquake. Pre-earthquake imagery from April 19, 2007 and April 30, 2008 were used along with post-earthquake imagery collected on May 16, 2008 and May 23, 2008. Composite pre- and post-event images are shown in Fig. 1. The pre-earthquake imagery is free of clouds, while a significant amount of cloud cover is found in the post-earthquake imagery, ranging from 27 to 55% for each scene. The cloud cover is mostly situated over the alluvial plain to the east of the fault rupture zone, although it does cover a significant area over the fault rupture itself.
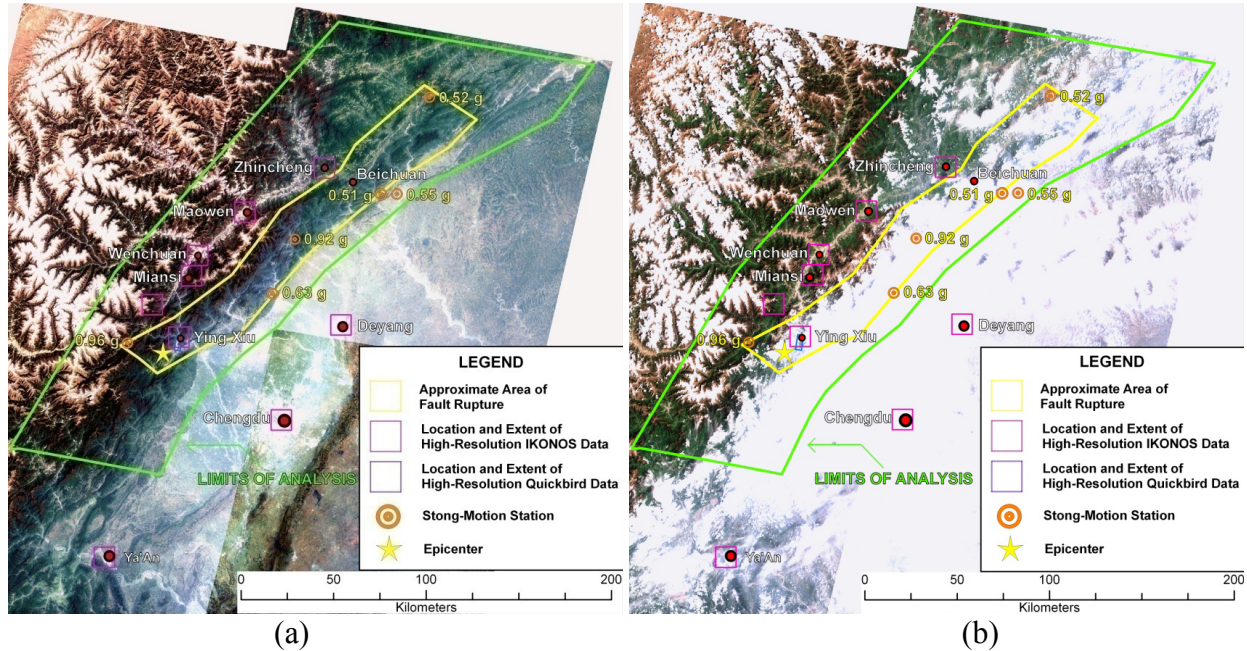

(a)	(b)

Figure 1.   (a) Pre-event and (b) post-event LANDSAT true-color imagery for the area affected by the 2008 Wenchuan earthquake. Locations of high-resolution imagery also shown.

The Enhanced Thematic Mapper Plus (ETM+) sensor on LANDSAT7 collects data in eight spectral bands at different resolutions. Bands 1 through 5 represent blue (wavelength 0.45-0.52 μm), green (0.52 – 0.60 μm), red (0.63- 0.69 μm), near infrared (0.77-0.90 μm), and mid-infrared (1.55-1.75 μm) wavelengths, and are collected at 30 m resolution. Bands 6 and 7 are the thermal infrared (10.4 - 12.5 μm) and short wave infrared (2.09-2.35 μm) bands and are collected at 60 m and 28.5 m resolution, respectively. Band 8 is the panchromatic band (0.52-0.90 μm), which represents a larger range of wavelengths, and is collected at 14.25 m resolution.

High resolution imagery from the Quickbird (QB) and IKONOS (IK) sensors was obtained for some localized areas in the region (Fig. 1). Pre- and post-event QB imagery was obtained for the area around and immediately south of the town of Ying Xiu in the epicentral area (Fig. 1), which allowed change detection analysis to be performed using high-resolution data. The pre-event QB data was collected on June 26, 2005 and the post event data was collected June 3, 2008. Both the pre- and post-event datasets are almost entirely cloud free, making them ideal for change detection analysis. Post-event high resolution imagery, without

any accompanying pre-event imagery, was obtained over various locations (Fig. 1) and used for visual interpretation of landslides.

The QB and IK sensors acquire panchromatic data (a single band between 0.45-0.90 μm, usually displayed as gray-scale) at high resolution (0.6 m for QB, 1.0 m for IK), as well as multispectral data at lower resolution (2.8 m for QB, 4.0 m for IK). The multispectral bands represent blue (0.45-0.52 μm), green (0.52-0.60 μm), red (0.63-0.69 μm), and near infrared (0.76-0.90 μm). Although the multispectral data are collected at a lower resolution, they can be fused with the higher resolution panchromatic data to produce spatially enhanced color images, called pan-sharpened images.

Change Detection Analysis

Earthquake-induced landslides generally correspond with areas of stripped vegetation on slopes that expose bare rock, soil, and debris. Change detection involves the identification of major changes between pre- and post-earthquake images. Commonly used change detection methods include image differencing, image-to-image correlation, and image ratioing. These techniques are performed on one or more spectral bands, and the bands are selected to best elucidate the type of change specific to the application.

Band selection for this study involved identifying which band best exhibited large changes in reflectance caused by either the removal of vegetation or the exposure of bare earth. Fig. 2 shows the reflectance of vegetation and soil at different wavelengths. In the visible light portion of the electromagnetic spectrum, the reflectance of soil is 5 to 10 percentage points larger than that of vegetation. The reflectance of soil is about 20 percentage points smaller than vegetation in the near-infrared (NIR) band, and 20 percentage points larger in the mid-infrared (MIR) band. These comparisons indicate that the removal of vegetation and exposure of bare earth caused by landslides causes the reflectance to increase in the visible light bands, to decrease in the NIR band, and to increase in the MIR band.
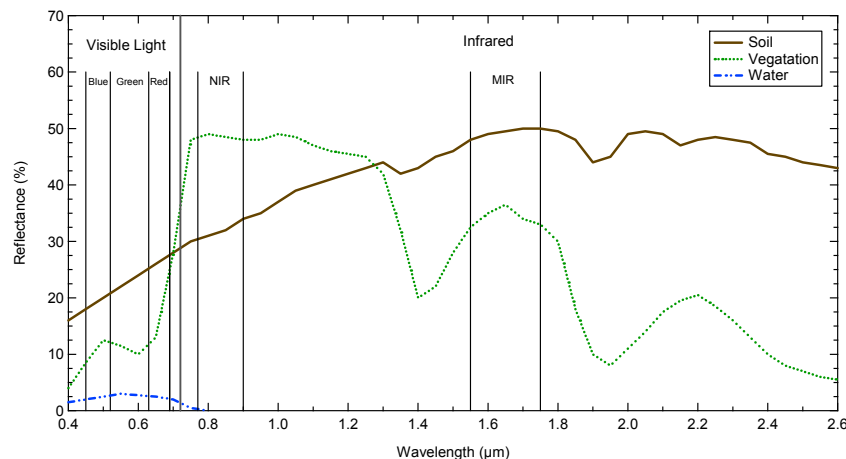

Figure 2.   Reflectance of bare soil, vegetation, and water versus spectral wavelength (modified from Lillesand et al. (2004)).

A test region near Miansi (Fig. 1) with prolific landsliding was used to initially assess the best band for use in the change detection. Comparisons between the visually observed landslides

and changes in each band indicated that the red band was the most sensitive to changes associated with landslides and was not significantly affected by seasonal changes in vegetation structure. However, another complicating factor was the cloud cover and haze in the LANDSAT imagery. The shorter wavelength of the red band is more affected by these atmospheric conditions, as compared to longer wavelength bands such as MIR. To minimize the area of affected by cloud cover and haze, the MIR band was used in the change detection analysis using the LANDSAT imagery. Because cloud cover was not an issue in the QB data over Ying Xiu, the red band was used in these analyses.

Several processing steps were incorporated into the change detection analysis (Carr 2009). First, the MIR data were converted from digital numbers (DN) to reflectance based on the sun angle and earth-sun distance at acquisition. The reflectance-converted scenes were stitched together to create a single pre-event image and a single post-event image. Clouds were manually masked out of the post-earthquake MIR data so their presence would not affect the analysis. The same areas were also masked out of the pre-earthquake MIR data. The final area of analysis, after cloud removal, was 15,709 km^2. Although the imagery was radiometrically corrected, differences in reflectances between the images are still present due to factors such as seasonal changes in vegetation and differences in sun illumination. To reduce the brightness contrasts between the images, the post-earthquake imagery was histogram matched to the pre-earthquake imagery. Histogram matching uses the histogram of the data in one image to stretch the data in the other image. The result is a similar brightness distribution in both images.

Change detection was based on the difference in MIR reflectances of the pre-earthquake and post-earthquake data for each individual pixel ($MIR_{POST} - MIR_{PRE}$). To identify an appropriate threshold for change, changes in reflectance were divided into classes ranging from $\leq$ -0.30 to > +1.00. For landslides, the reflectance in the MIR band should become larger (Fig. 2), thus positive changes are of most significance. For positive changes, the change classes were defined at threshold increments of 0.02 (i.e., 0.00 to +0.02, +0.02 to +0.04, etc.). The change detection thresholds were used to create difference maps, which show all areas corresponding to the particular change detection thresholds. The best threshold for landslide identification was found by visually comparing the change detection difference map and the post-event multispectral data for each threshold considered. Figure 3 shows areas of identified landslides based on the threshold of > +0.10 for the test region near Miansi. Thresholds smaller than +0.10 greatly overestimated the presence of landslides and also incorrectly identify terraced agricultural areas in the northwest portion of the imagery as landslides. Larger thresholds, such as +0.14, tended to omit or minimize the size of many landslides, although the larger threshold reduced errors between terraced agricultural areas and landslides. This visual interpretation resulted in a threshold of > +0.10 being selected to provide the best overall approximation of the landslide distribution.

Change detection was also performed using pre- and post-event QB data obtained for the area around Ying Xiu. Change detection with high resolution data can be used to find not only landslides, but urban damage as well. Additionally, both the pre- and post-event datasets are almost entirely cloud free, which eliminated many of the problems encountered during the LANDSAT change detection analysis. Change detection was performed using the red band, as this band is generally insensitive to seasonal changes in vegetation and exhibits large changes in reflectance between bare soil and vegetation (Fig. 2). Change detection was performed on data converted from DN format to radiance. Histogram matching was not performed, as the large landslide concentrations caused the brightness distributions to be considerably different between

scenes. Initial change detection classes ranged from changes in radiance from < -0.30 to > +13.75, with classes representing positive change defined every +0.25. Visual interpretation of the computed change detection maps resulted in a threshold of > +2.25 being selected. Figure 4 shows a portion of the QB post-event data overlain with earthquake change defined based on the threshold of >+2.25. Thresholds of less than +2.25 tended to greatly overestimate the area of earthquake change. Larger change thresholds performed a satisfactory assessment of damage, but missed some of the edges of the landslides, very small landslides, and also tended to slightly underestimate urban damage. Thus, a threshold of > +2.25 was used to identify earthquake-induced change.
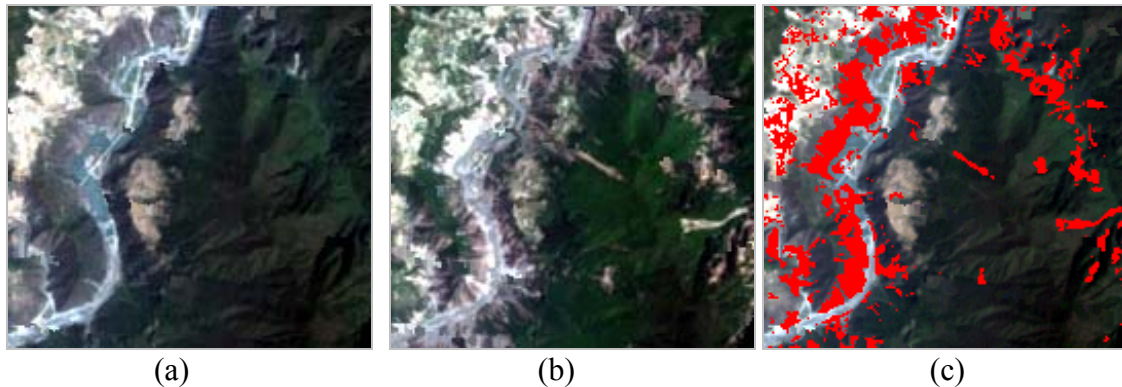

| (a) | (b) | (c) |

Figure 3. (a) Pre-event true color LANDSAT imagery near Miansi, (b) post-event true color LANDSAT imagery of same area, and (c) landslides identified using a change-detection threshold of > +0.10 for the MIR band. Scene size is 11 km by 11 km.
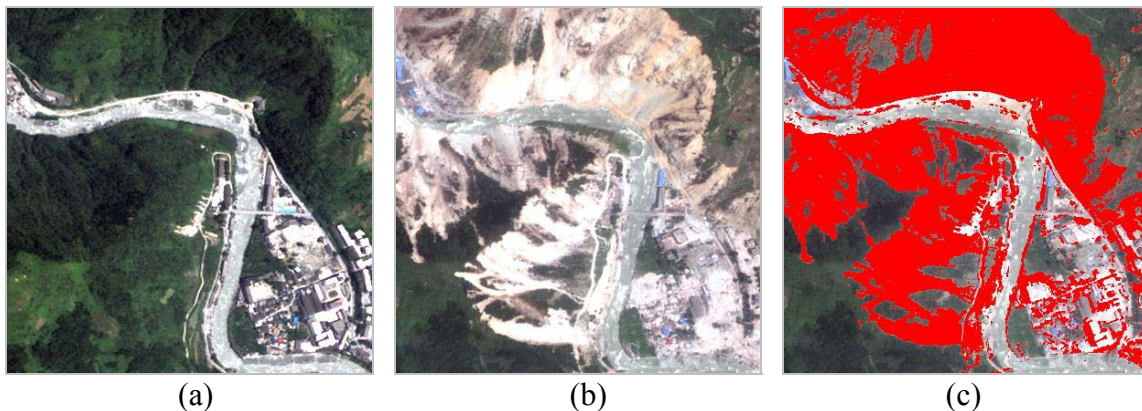

| (a) | (b) | (c) |

Figure 4. (a) Pre-event true color QB imagery, (b) post-event true color QB imagery, and (c) landslides/urban damage identified using a change detection threshold of >+2.25 for the red band. Scene size is 0.96 km by 0.96 km.

Landslide Distributions from Satellite Imagery

Results from LANDSAT Imagery

The change detection procedures discussed previously were used to develop landslide maps of the area affected by the Wenchuan earthquake. Figure 5 shows the post-event LANDSAT imagery with the landslides identified from the change detection analysis shown in

red. Note that significant sections of the affected area are covered in clouds and could not be analyzed. For the areas that could be analyzed, 436 km^2 of landslides were identified, with landslide concentrations greatest in the river valley directly north-northeast of the epicenter along the fault rupture zone. High landslide concentrations are observed north to approximately the Wenchuan area, after which the concentrations are reduced. Landslides are also observed in the northern portions of the analyzed area, such as around the town of Zhincheng and areas to the northeast of Beichuan.

Based on field observations, it is known that high landslide concentrations are present beneath the cloud cover along the fault rupture zone. For example, the town of Beichuan was heavily damaged by landslides, but this area is not visible in this imagery due to cloud cover. Additionally, the steep topography typical of the region extends beneath the cloud cover along the entire fault rupture zone, making this area susceptible to landslides. Therefore, the landslide concentrations shown in Fig. 5 should be considered incomplete due to the cloud cover.

A zone of fewer landslides is located between the Ying Xiu and Mountain Area scenes (Fig. 5), with zones of significant landslides to the east and west. This area corresponds to a geologic unit identified as a "fractured horizon" (Berman 2008), consisting of sedimentary rocks including shale, limestone, and sandstone. The geologic units located east of this area consist of crystalline rocks such as granite, and geologic units to the west consist of metamorphic rocks such as schist and griotte. The descriptions of these geologic units do not explain the different concentrations of landslides. These areas will be discussed further later in this paper.
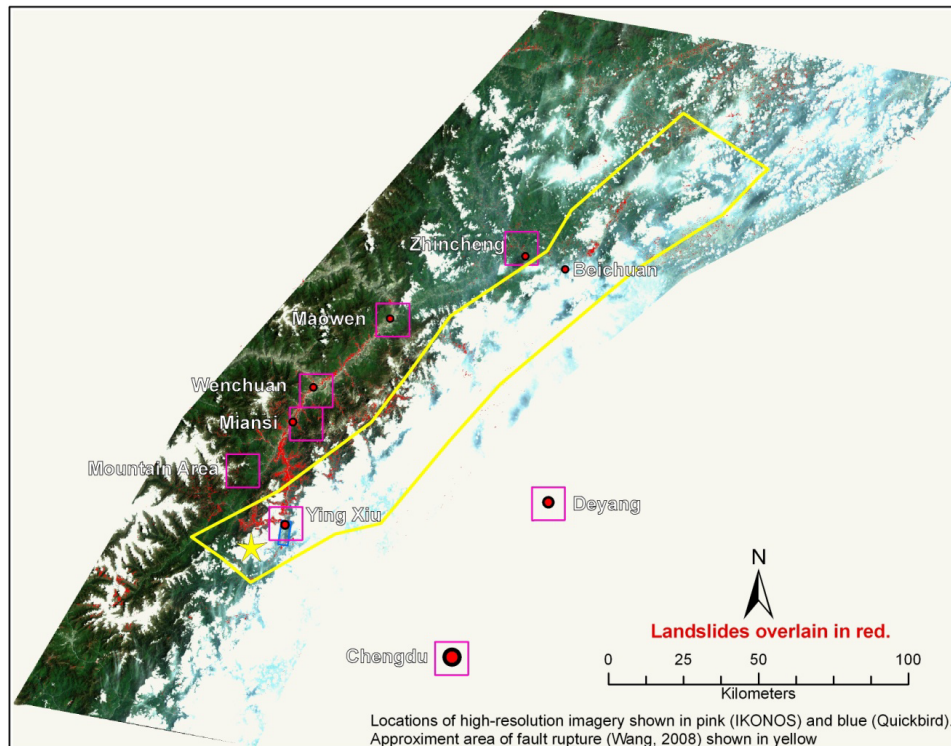

Figure 5. Spatial extent of landslides obtained from change detection analysis using LANDSAT imagery.

Results from High-Resolution Imagery

  Post-earthquake, high-resolution imagery was available from the IKONOS (IK) and Quickbird (QB) sensors for areas of Zhincheng (IK), Maowen (IK), Wenchuan (IK), Miansi (IK), a Mountain Area (IK) and Ying Xiu (IK and QB). Pre-earthquake, high-resolution imagery was available only for Ying Xiu (QB). The QB scenes over Ying Xiu represent a different spatial extent than the IK scene. Visual interpretation of the five IK scenes and the one QB scene were performed to identify landslides and urban damage. Change detection was also performed using the QB imagery for Ying Xiu. The locations of these scenes are shown in Fig. 5.

  Table 1 lists the total area of earthquake damage/change identified from the visual interpretation of the high resolution data and from the LANDSAT change detection analysis. For 6 of the 7 scenes, the LANDSAT analysis predicted a damage area less than or equal to the area identified in the visual interpretation. In only one case did the LANDSAT analysis predict a larger area of damage than visual interpretation. For four of the seven scenes (Maowen, Miansi, Mountain Area, and Wenchuan), the damage area identified by the LANDSAT analysis was with +/-30% of the area identified in the high-resolution imagery. In the remaining three scenes (Ying Xiu (IK), Ying Xiu (QB), and Zhincheng), the LANDSAT analysis identified 40 to 60% less earthquake change. The tendency for the LANDSAT analysis to underestimate the landslide areas is due to differences in the character in the exposed soil for differences part of the imagery, as well as some issues with shadows and haze. Identifying different thresholds for different parts of the imagery would have improved the LANDSAT analysis, but would have increased the time to perform the analysis.

Table 1. Earthquake change areas from visual identification of high resolution imagery and from LANDSAT change detection.

Scene /Data Type	Earthquake Change Area (km^2)		Ratio
	Visual ID from High Res. Imagery	LANDSAT Change Detection	(LANDSAT /High Res.)
Maowen (IK)	5.0	3.8	0.76
Miansi (IK)	15.7	15.8	1.01
Mountain Area (IK)	1.4	1.4	1.00
Wenchuan (IK)	14.0	18.3	1.31
Ying Xiu (IK)	17.8	10.5	0.59
Ying Xiu (QB)	5.4	2.3	0.43
Zhincheng (IK)	5.1	2.5	0.49

  Change detection analysis was also performed using the QB imagery for Ying Xiu. Fig. 6 shows the results of the change detection analysis. Overall, the landslide distribution is very similar to the results of the visual interpretation of the scene (Carr 2009); however the change detection analysis identified many small landslides across the image that were not visually identified. These landslides appear to have been overlooked in the visual analysis because of their small size, but the high-resolution change detection analysis was able to identify them.

Some overestimation of landslide area was noticed in the change detection results in the northern portions of the imagery, while the change detection results in the southern portions provided a more accurate assessment than visual interpretation. Extensive urban damage in the town of Ying Xiu was also identified by the change detection analysis. The impounded water located in the southern portion of the imagery was identified in the change detection analysis, although this area does not represent landslide. This result illustrates the importance of validating change detection analyses with visual interpretation of the imagery.

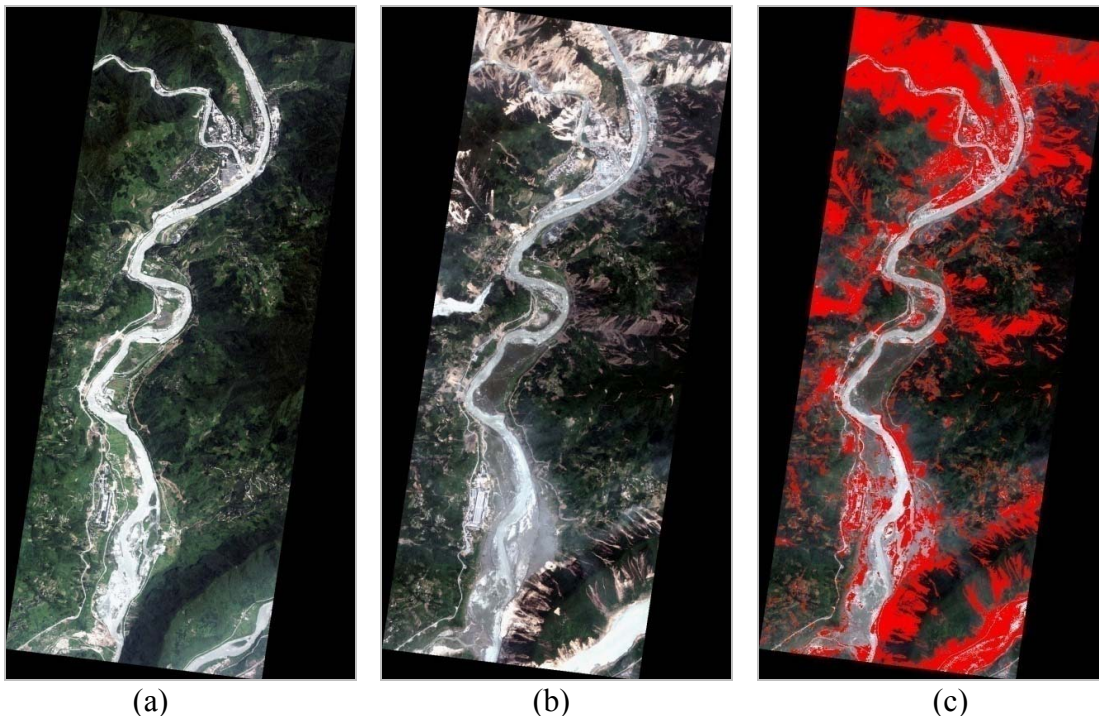<center>(a)   (b)   (c)</center>

Figure 6. (a) Pre-earthquake imagery, (b) post-earthquake imagery, and (c) change detection results for QB imagery of Ying Xiu (shown in red). Scene size is 3.2 km by 8.1 km.

Relationship between Landslides and Topography

The LANDSAT analysis revealed an interesting pattern of landslides north and west of Ying Xiu, with large landslide frees areas adjacent to areas with significant landslides (Fig. 5). These areas are shown in more detail in Fig. 7. Landslide Free Area-1 is a strip of area west of the fault rupture that experienced almost no landslides. This area is directly west of large concentrations of landslides near Ying Xiu (Landslide Area-East). Landslides are also found to the west (Landslide Area-West), although in smaller concentrations than near Ying Xiu. The geologic map of the Sichuan province (Berman 2008) shows that Landslide Free Area-1 consists of fractured sedimentary rocks, while schist and griotte are found in the Landslide Area-West and granite is found in the Landslide Area-East. Considering the geology of the area and the large ground shaking expected close to the fault rupture, landslides should have occurred in all three of these areas.

Similar discrepancies in landslide concentration are found to the north of Ying Xiu. Landslide Area-Miansi and Landslide Free Area-2 are both located a similar distance from the fault rupture, about 10 to 15 km, but Landslide Area-Miansi exhibited extensive landslides while

Landslide Free Area-2 did not. Both areas are located in the same geologic unit of fractured sedimentary rocks. The observations of landslides in these five areas were investigated using topography data.

The topography data represented data from the Shuttle Radar Topography Mission (SRTM), which consists of 3 arc-second radar elevation data across most of the world. The 3 arc-second resolution data translates to a spatial resolution of roughly 76 m EW by 92 m NS in the area affected by the Wenchuan earthquake. Gap-filled SRTM data was obtained from the Consultative Group on International Agricultural Research Consortium for Spatial Information (CGIAR-CSI 2008), which maintains a free database of SRTM data for most of the earth.
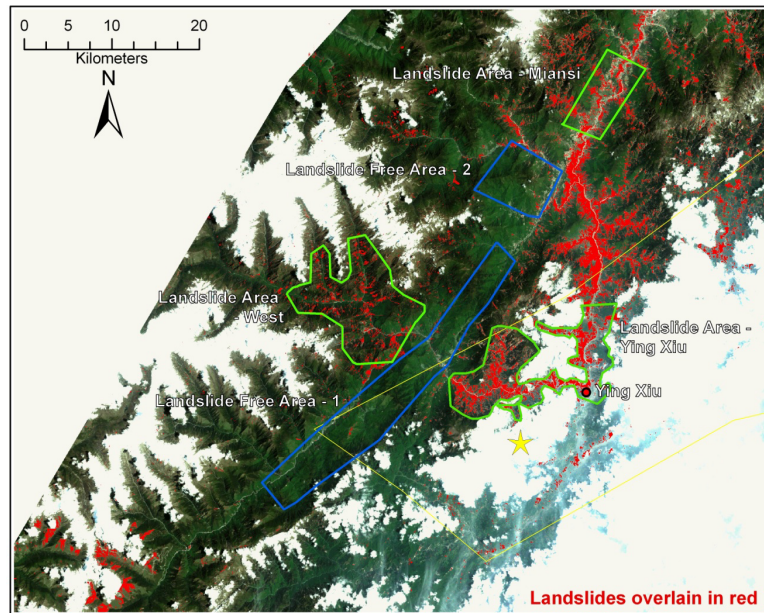

Figure 7. Areas of different landslide concentrations.

The SRTM elevation data was used to compute slope angles for each of the areas outlined in Fig. 7. The resulting slope angle distributions are shown in Fig. 8. The distribution of slope angles for Landslide Area-Ying Xiu and Landslide Area-West are nearly identical, with median slope angles of about 40°. In comparison, Landslide Free Area-1 has a median slope angle of 30° and few slopes steeper than 40°, thus the area is generally much flatter. Landslides cover 0.4% of the ground surface in Landslide Free Area-1, while the landslide density was 28% and 10% in Landslide Area-Ying Xiu and Landslide Area-West, respectively. In this case, the presence of landslides can be directly correlated to the distributions of slope angle in the areas.

Comparison of the slope angles from Landslide Area-Miansi and Landslide Free Area-2 (Fig. 8) shows that Landslide Area-Miansi exhibits slightly steeper slopes. The median slope angle is 34° for Landslide Free Area-2, while it is 36° for Landslide Area-Miansi. While the slope angles for Landslide Free Area-2 are shifted slightly to the left of that from Landslide Area-Miansi, the difference is not as great as observed other analyzed areas. Landslide concentrations differ by a factor of 10 for these two areas, with 20% of the ground surface covered in landslides in Landslide Area-Miansi and less than 2% in Landslide Free Area-2. It is possible that the considerably larger landslide concentration in Landslide Area-Miansi is caused by the slightly steeper distribution of slopes. This area is also located along a river valley, where the highest concentrations were found and may have influenced the distribution of landslides.

The difference may also be caused by differences in ground shaking, but data is not available to investigate this effect.
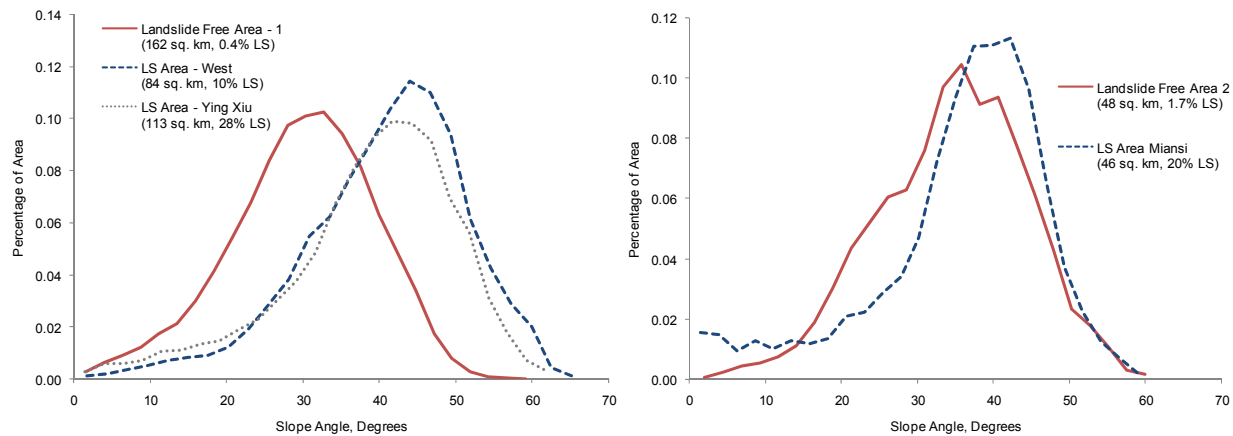

Figure 8. Distribution of slope angles for areas with different landslide concentrations.

Conclusions

This paper uses satellite imagery to investigate the landslides caused by the 2008 Wenchuan earthquake in China. The study demonstrates that moderate resolution LANDSAT imagery can be used to rapidly identify landslide distributions using change detection analysis. While the LANDSAT results lack some detail, they provide a good sense of the landslide distribution across the entire area affected by the earthquake. High-resolution imagery provides more detail regarding the landslides, but cannot quickly identify the landslides across the large area affected by the earthquake. Landslide identification via satellite imagery will play an important role in developing datasets of earthquake-induced landslides for use in validating methodologies of earthquake-induced landslide prediction.

Acknowledgments

References

Berman, L., 2008. "Sichuan Geological Map – RASTER." *China Earthquake Geospatial Research Portal*. <http://cegrp.cga.harvard.edu/content/sichuan-geological-map-raster>

Carr, L.P., 2009. The Application of Remote Sensing for Mapping Earthquake-Induced Landslides from the 2008 Wenchuan, China and 2004 Niigata-Ken Chuetsu, Japan Earthquakes. *M.S. Thesis,* University of Texas at Austin.

CGIAR-CSI 2008. "CGIAR-CSI SRTM 90m Digital Elevation Database." *The CGIAR Consortium for Spatial Information.* <http://srtm.csi.cgiar.org/>

Lillesand, T.M., Kiefer, R.W., and Chipman, J.W., 2004. *Remote Sensing and Image Interpretation,* John Wiley and Sons, Inc., New York, NY.